An effective technique for increasing capacity and improving bandwidth in 5G narrow-band internet of things

Abdulwahid Mohammed[1], Hassan Mostafa[2,3], Abdelhady Abdelazim Ammar[1]

[1]Department of Electronics and Communication Engineering, Al-Azhar University, Cairo, Egypt
[2]Department of Electronics and Communication Engineering, Cairo University, Giza, Egypt
[3]Department of Electronics and Communication Engineering, University of Science and technology, Giza, Egypt

Article Info

ABSTRACT

In recent years, the wireless spectrum has become increasingly scarce as demand for wireless services has grown, requiring imaginative approaches to increase capacity within a limited spectral resource. This article proposes a new method that combines modified symbol time compression with orthogonal frequency division multiplexing (MSTC-OFDM), to enhance capacity for the narrow-band internet of things (NB-IoT) system. The suggested method, MSTC-OFDM, is based on the modified symbol time compression (MSTC) technique. The MSTC is a compressed waveform technique that increases capacity by compressing the occupied symbol time without losing bit error rate (BER) performance or data throughput. A comparative analysis is provided between the traditional orthogonal frequency division multiplexing (OFDM) system and the MSTC-OFDM method. The simulation results show that the MSTC-OFDM scheme drastically decreases the symbol time (ST) by 75% compared to a standard OFDM system. As a result, the MSTC-OFDM system offers four times the bit rate of a typical OFDM system using the same bandwidth and modulation but with a little increase in complexity. Moreover, compared to an OFDM system with 16 quadrature amplitude modulation (16QAM-OFDM), the MSTC-OFDM system reduces the signal-to-noise ratio (SNR) by 3.9 dB to transmit the same amount of data.

Corresponding Author:

Abdulwahid Mohammed
Electronics and Communication Engineering Department, Al-Azhar University
Nasr Street, Permanent Camp, Cairo 11651, Egypt
Email: abdulwahid.21@azhar.edu.eg

1. INTRODUCTION

Over the past few years, the internet of things (IoT) has evolved tremendously. The IoT provides a wide range of possibilities for novel applications to enhance our lives [1]. The number of connected devices is constantly increasing, and new IoT applications in vehicles, transport, the electric grid, agriculture, metering, and other fields have developed [2]. In particular, IoT enables humans to live in a smarter environment than ever before. For instance, residents all around the world receive personalized urban services on a continuous, automated, and collaborative basis [3]. IoT devices have emerged in different environments, such as smart grids [4], industrial automation [5], smart cities, healthcare, and home appliances [6]. According to the global system for mobile communications association (GSMA), IoT connections forecast (5) and Ericsson mobility's report (4), both of which were issued in June 2020 (these two reports include the impact of the coronavirus disease (COVID-19) epidemic on the IoT industry), the total number of IoT device connections is expected to

approach over 75 billion among all IoT markets by 2025 [7]. The smart home, consumer electronics, wearables, and smart vehicle sectors are expected to be the primary drivers of development in consumer IoT [7].

A variety of low power wide area (LPWA) systems have evolved to handle this massive data need [8]. In addition to the wide coverage, low power consumption, and large number of users, these technologies also provide a low level of device complexity [9], [10]. There are several standardization committees working on standardizing LPWA technology, including IEEE, 3GPP, and others [2]. LPWA can employ cellular or non-cellular wireless technologies. Cellular technologies include machine type communication (MTC), enhanced machine type communication (eMTC), and narrow-band internet of things (NB-IoT) [11], whereas non-cellular technologies include long range (LoRa), ZigBee, Bluetooth, Z-Wave, and others [12]–[14]. With the explosive growth of 5G new radio technologies, industry and academia are focusing their efforts on enhanced mobile broadband (eMBB), massive machine-type communications (mMTCs), and ultra-reliable low latency communications (URLLCs) [15]. To meet the 5G vision, it is required to not only make substantial advancements in new wireless technologies, but also to consider the harmonic and equitable coexistence of diverse networks, and the compatibility of 4G and 5G systems [16].

The rest of this paper is organized as follows. Section 2 summarizes the related work and contribution. Section 3 describes the overall mathematical model of the proposed system. The simulation results and comments are presented in section 4. This study is summarized in section 5 by outlining the advantages of the proposed technique.

2. RELATED WORK AND CONTRIBUTION

The third generation partnership project (3GPP) produced the NB-IoT radio technology standard for cellular devices and services [17]. As opposed to conventional multi-carrier systems, NB-IoT typically uses low-order modulation techniques like binary phase shift keying (BPSK) and fewer sub-carriers. The drawback of NB-IoT is that it cannot be used for critical systems due to its constrained bandwidth and transmission rate [18]. Therefore, this article focuses on increasing data rates and improving performance within the constrained NB-IoT bandwidth.

Xu and Darwazeh [19] proposed an NB-IoT architecture based on a sophisticated signal waveform known as non-orthogonal spectrum efficient frequency division multiplexing (SEFDM). Compared with OFDM, the developed waveform might enhance the data rate without requiring extra bandwidth. According to the simulation results, the suggested waveform might enhance data rates by 25% when compared to the OFDM signal waveform. However, the non-orthogonality of the sub-carriers may lead to inter-carrier interference (ICI), requiring additional power consumption on the receiver side. Since the signal processing is done at the base stations, it is appropriate for the up-link channel [19]. But this is not practicable since it requires additional processing at the down-link channels.

Xu and Darwazeh [20] described solutions for NB-IoT employing fast orthogonal frequency division multiplexing (Fast-OFDM), as this technique shows its advantages compared to the standard orthogonal frequency division multiplexing (OFDM). When compared to a typical OFDM system, fast-OFDM reduces the space between sub-carriers by 50% and avoids bit error rate (BER) degradation. As a result, it doubles the number of connected devices by reducing the utilized bandwidth of each device without affecting BERperformance. However, Fast-OFDM may cause carrier frequency offset (CFO) due to lowering sub-carrier spacing.

Xu *et al.* [21] employed non-orthogonal multi-carrier SEFDM wave-forms for single and multiple-antenna systems and demonstrate how these wave-forms may improve down-link (DL) bandwidth by 11% when compared to NB-IoT. The results demonstrated that enhanced NB-IoT (eNB-IoT) has the same efficiency as NB-IoT in both single and multiple antennae for modulation schemes such as quadrature amplitude modulation (4QAM and 8QAM). However, NB-IoT outperforms eNB-IoT in higher-order modulation formats such as 16QAM.

Liu and Darwazeh [18] proposed a new signaling technique for NB-IoT mobile systems based on the Fast-OFDM scheme coupled with a time orthogonal Hilbert transform (HT) pair (HT-Fast-OFDM), which quadruples the data rate by applying two orthogonal methods: the Fast-OFDM scheme combined with the time orthogonal hilbert transform (HT) pair. According to their simulation studies, the HT-Fast-OFDM system offers four times the data rate compared with an OFDM system using the same modulation technique (BPSK) and utilizing the same bandwidth. However, because of the reduced sub-carrier spacing, F-OFDM may suffer from a carrier frequency offset (CFO). Furthermore, the combination of two orthogonal techniques increases

the complexity of the HT-Fast-OFDM system.

In this study, the modified symbol time compression with orthogonal frequency division multiplexing (MSTC-OFDM) is suggested as a promising and effective system for 5G and beyond for the following reasons: i) increase the data rate four times compared with a typical OFDM system; ii) using one-dimensional modulation leads to lower power consumption; iii) as opposed to Fast-OFDM in [20], it does not cause a mismatch in the sampling rate or CFO since the space between the sub-carriers is not reduced; iv) enhances system performance by further keeping the system from degrading in BER; and v) the MSTC-OFDM outperforms the HT-Fast-OFDM in terms of complexity. Furthermore, unlike the HT-Fast-OFDM system in [18], the MSTC-OFDM system maintains the same spacing between the sub-carriers, making it more robust against CFO and inter-carrier interference.

3. SYSTEM MODEL

The symbol time compression (STC) technique is initially presented in [22], where it compresses the symbol time to half and saves 50% of bandwidth. This article suggests the MSTC technique, which reduces the used bandwidth to a quarter while saving 75% of symbol time. Moreover, using MSTC does not cause deterioration in BER, as will be demonstrated in further detail in section 4. The MSTC technique is applied on the transmitter side, while the modified symbol time extension (MSTE) technique is employed on the receiver side. The mathematical model can be divided into three parts as: i) the MSTC mathematical model at the transmitter side; ii) the MSTE mathematical model at the receiver side; and iii) the system model of the suggested system, MSTC-OFDM.

3.1. MSTC system model

On the transmitter side, the MSTC scheme is applied through two procedures. The spreading procedure is carried out first, and subsequently the combining process. Two comparable units are joined to create the MSTC technique. The output of the second unit is multiplied by "j" to obtain the imaginary component, which is then added to the output of the first unit to produce the complex output X_c, as depicted in Figure 1.
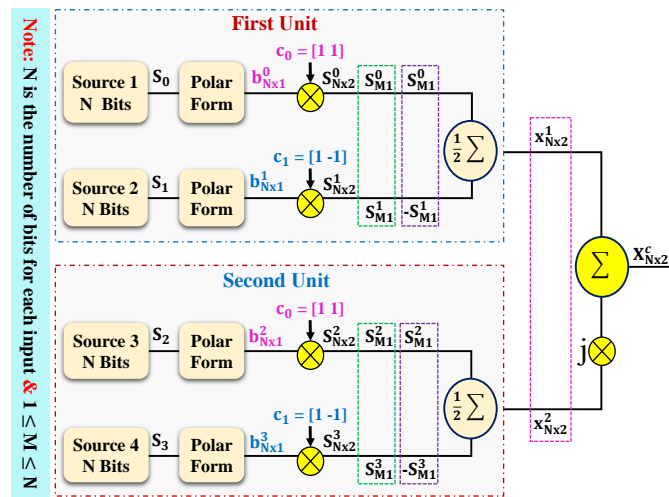

Figure 1. Block diagram of M-STC technique

Figure 1 displays the block diagram of the MSTC technique. First, the input data (S_0, S_1, S_2, and S_3) is converted to the polar form ((b^0_{Nx1}, b^1_{Nx1}, b^2_{Nx1}, and b^3_{Nx1}). The polar form for the first unit is (b^0_{Nx1} and b^1_{Nx1}), and for the second unit is (b^2_{Nx1} and b^3_{Nx1}). The polar form for the two units is expressed as (1):

$$b^0_{N\times 1} = \begin{bmatrix} b^0_{11} \\ . \\ b^0_{N1} \end{bmatrix}, b^1_{N\times 1} = \begin{bmatrix} b^1_{11} \\ . \\ b^1_{N1} \end{bmatrix}, b^2_{N\times 1} = \begin{bmatrix} b^2_{11} \\ . \\ b^2_{N1} \end{bmatrix} b^3_{N\times 1} = \begin{bmatrix} b^3_{11} \\ . \\ b^3_{N1} \end{bmatrix} \tag{1}$$

Second, the polar form is spread using the Walsh code (c), which is constructed using the Hadamard matrix (H). The Hadamard matrix is a symmetric square matrix, and each row of the Hadamard matrix is orthogonal to every other row. The (2×2) Hadamard matrix is used in this article and is given as (2) [23]:

$$H_{2x2} = \begin{bmatrix} 1 & 1 \\ 1 & -1 \end{bmatrix} \tag{2}$$

The Hadamard matrix represents a different Walsh code and each row or column of this matrix represents a different Walsh code. The two spreading Walsh codes are given as (3) [24]:

$$c_0 = \begin{bmatrix} 1 & 1 \end{bmatrix} \quad and \quad c_1 = \begin{bmatrix} 1 & -1 \end{bmatrix}. \tag{3}$$

The spread data is obtained by multiplying the polar data (b_{Nx1}^0, b_{Nx1}^1, b_{Nx1}^2 and b_{Nx1}^3) by the Walsh codes (c_0 and c_1) as (4):

$$S_{N \times 2}^0 = b_{N \times 1}^0 \times c_0 = \begin{bmatrix} S_{11}^0 & S_{12}^0 \\ S_{N1}^0 & S_{N2}^0 \end{bmatrix} = \begin{bmatrix} b_{11}^0 & b_{11}^0 \\ b_{N1}^0 & b_{N1}^0 \end{bmatrix}, S_{N \times 2}^1 = b_{N \times 1}^1 \times c_1 = \begin{bmatrix} S_{11}^1 & S_{12}^1 \\ S_{N1}^1 & S_{N2}^1 \end{bmatrix} = \begin{bmatrix} b_{11}^1 & -b_{11}^1 \\ b_{N1}^1 & -b_{N1}^1 \end{bmatrix},$$
$$S_{N \times 2}^2 = b_{N \times 1}^2 \times c_0 = \begin{bmatrix} S_{11}^2 & S_{12}^2 \\ S_{N1}^2 & S_{N2}^2 \end{bmatrix} = \begin{bmatrix} b_{11}^2 & b_{11}^2 \\ b_{N1}^2 & b_{N1}^2 \end{bmatrix} S_{N \times 2}^3 = b_{N \times 1}^3 \times c_1 = \begin{bmatrix} S_{11}^3 & S_{12}^3 \\ S_{N1}^3 & S_{N2}^3 \end{bmatrix} = \begin{bmatrix} b_{11}^3 & -b_{11}^3 \\ b_{N1}^3 & -b_{N1}^3 \end{bmatrix} \tag{4}$$

where $S_{N \times 2}^0$ and $S_{N \times 2}^1$ are the spread data of the first unit, whereas $S_{N \times 2}^2$ and $S_{N \times 2}^3$ are the spread data of the second unit. The combining process is then applied to the spread data for both the first and second units after the spreading procedure. The spread data $S_{N \times 2}^0$ and $S_{N \times 2}^1$ are joined in the first unit to produce the combined data x_{Nx2}^1. Similarly, in the second unit, the spread data $S_{N \times 2}^2$ and $S_{N \times 2}^3$ are grouped to provide the combined data x_{Nx2}^2. The combining process for the first and second units is given as (5):

$$x_{Nx2}^1 = \tfrac{1}{2} \begin{bmatrix} (S_{M1}^0 + S_{M1}^1) & (S_{M1}^0 - S_{M1}^1) \end{bmatrix}, \quad x_{Nx2}^2 = \tfrac{1}{2} \begin{bmatrix} (S_{M1}^2 + S_{M1}^3) & (S_{M1}^2 - S_{M1}^3) \end{bmatrix} \tag{5}$$

where x_{Nx2}^1 is the combining data for the first unit, x_{Nx2}^2 is the combining data for the second unit, $1 \leq M \leq N$, and N represents the input's bits. As displayed in Figure 1, the complex output X_c is created by adding the imaginary component, obtained by multiplying the output of the second unit by "j," to the first unit's output. The output of the MSTC technique is expressed as (6).

$$X_{Nx2}^c = x_{Nx2}^1 + jx_{Nx2}^2. \tag{6}$$

Figure 2 illustrates how the MSTC methodology employs the spread and combining procedures to compress the symbol time and increase the data rate. The MSTC approach delivers four bits per symbol time rather than one bit per symbol time. However, as will be demonstrated in Section 4, the BER obtained using the MSTC method is identical to the BER obtained using BPSK modulation. In Figure 2, we use four symbols to transfer four bits (b_1, b_2, b_3 and b_4). Each symbol time has a bit rate of R. The transmitted bits are multiplied by Walsh codes c_0 and c_1, as illustrated in Figure 2, to produce spread data as (7), (8):

$$S_{d1} = b_1 \times c_0 = \begin{bmatrix} b_1 & b_1 \end{bmatrix}, \qquad S_{d2} = b_2 \times c_1 = \begin{bmatrix} b_2 & -b_2 \end{bmatrix}, \tag{7}$$

$$S_{d3} = b_3 \times c_0 = \begin{bmatrix} b_3 & b_3 \end{bmatrix}, \qquad S_{d4} = b_4 \times c_1 = \begin{bmatrix} b_4 & -b_4 \end{bmatrix}, \tag{8}$$

where S_{d1}, S_{d2}, S_{d3}, and S_{d4} are spread data for the transmitted bits b_1, b_2, b_3 and b_4 respectively. The combining process of spreading data is defined as (9), (10):

$$C_{d1} = \begin{bmatrix} b_1^c & b_2^c \end{bmatrix} = \begin{bmatrix} (b_1 + b_2) & (b_1 - b_2) \end{bmatrix} \tag{9}$$

$$C_{d2} = \begin{bmatrix} b_3^c & b_4^c \end{bmatrix} = \begin{bmatrix} (b_3 + b_4) & (b_3 - b_4) \end{bmatrix} \tag{10}$$

It is clear from Figure 2 that the rate of combining data $C_{d1} = 2R$ and the rate of $C_{d2} = 2R$. The output of the MSTC technique is written as (11):

$$X_c = [x_1^c \quad x_2^c] = [(b_1^c + jb_3^c) \quad (b_2^c + jb_4^c)], \tag{11}$$

where X_c is the output of the MSTC technique. The data rate of X_c is 4R. Therefore, using the MSTC technology enhances capacity by compressing symbol time and sending data at a fourfold higher rate.
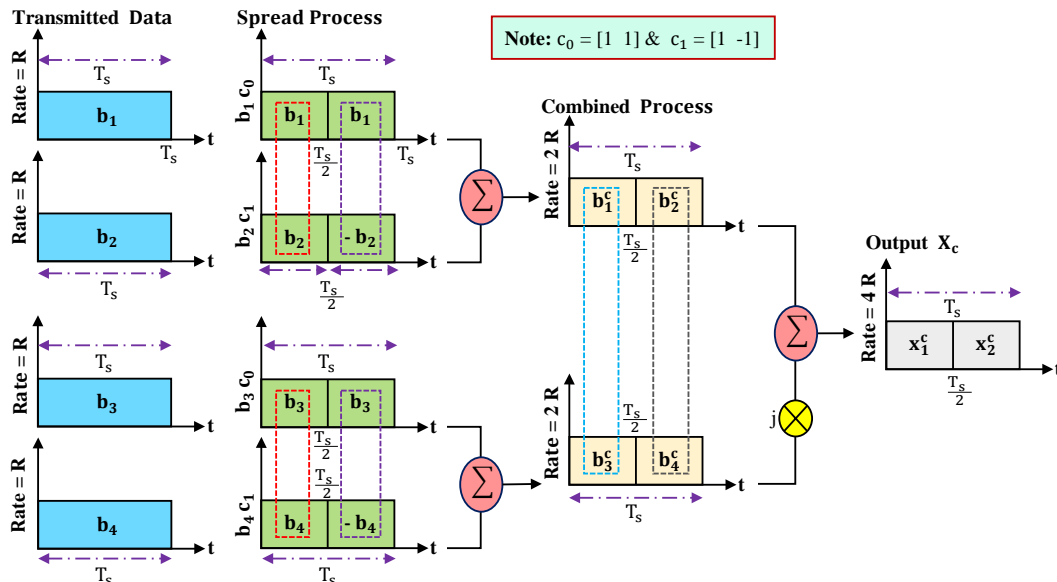

Figure 2. Illustrative example of the increasing data rate using the MSTC technique

3.2. MSTE system model

The mathematical analysis is explained in detail for the MSTE technique in this subsection. To reverse the procedures that the MSTC technique performed in the transmitter, the MSTE technique is employed at the receiver side. As indicated in Figure 3, the received signal ($Y_{2N\times1}^c = Y_{real} + jY_{imag}$) is divided into two parts: real (part 1) and imaginary (part 2). For the first unit, the real portion of the received signal is initially transformed to a Nx2 matrix in the following manner:

$$M_{N\times2}^R = \begin{bmatrix} Y_{11}^R & Y_{12}^R \\ & \cdot \\ Y_{N1}^R & Y_{N2}^R \end{bmatrix}. \tag{12}$$

The Walsh codes c_0 and c_1 are multiplied by (12) to disseminate data in the first unit as (13):

$$M_{N\times2}^{R_0} = M_{N\times2}^R \times c_0 = \begin{bmatrix} Y_{11}^R & Y_{12}^R \\ & \cdot \\ Y_{N1}^R & Y_{N2}^R \end{bmatrix}, \qquad M_{N\times2}^{R_1} = M_{N\times2}^R \times c_1 = \begin{bmatrix} Y_{11}^R & -Y_{12}^R \\ & \cdot \\ Y_{N1}^R & -Y_{N2}^R \end{bmatrix}. \tag{13}$$

where, c_0=[1 0 ; 0 1] and c_1=[1 0 ; 0 -1]. The combining process is applied to the spread data to produce the combined data. In (14) illustrates the process of combining data:

$$\underbrace{D_R^0}_{Nx1} = \frac{\sum_{i=1}^{N}\left(M_{i1}^{R_0} + M_{i2}^{R_0}\right) + 1}{2}, \qquad \underbrace{D_R^1}_{Nx1} = \frac{\sum_{i=1}^{N}\left(M_{i1}^{R_1} + M_{i2}^{R_1}\right) + 1}{2} \tag{14}$$
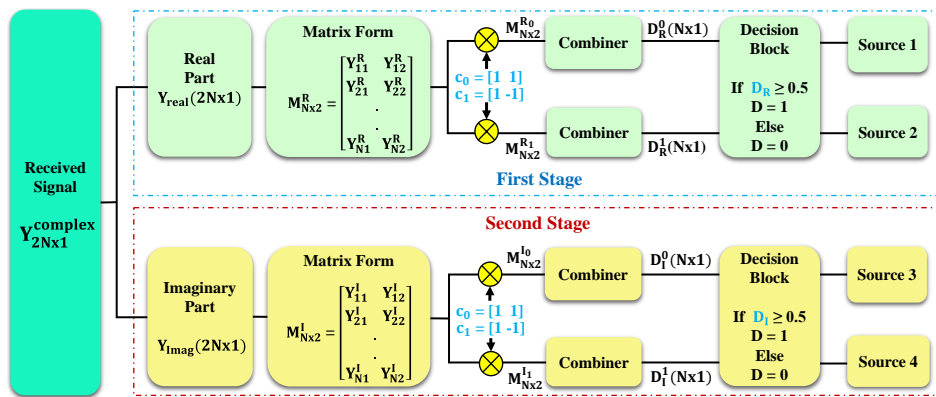
Figure 3. Block diagram of M-STE technique

Similarly, the second unit repeats all of the prior unit's steps. As a result, the imaginary portion of the received signal is expressed as (15):

$$M_{N \times 2}^{I} = \begin{bmatrix} Y_{11}^{I} & Y_{12}^{I} \\ & \cdot \\ Y_{N1}^{I} & Y_{N2}^{I} \end{bmatrix} \tag{15}$$

in (15) is multiplied by Walsh codes c_0 and c_1 to obtain the spread data in the second unit:

$$M_{N \times 2}^{I_0} = M_{N \times 2}^{I} \times c_0 = \begin{bmatrix} Y_{11}^{I} & Y_{12}^{I} \\ & \cdot \\ Y_{N1}^{I} & Y_{N2}^{I} \end{bmatrix}, \quad M_{N \times 2}^{I_1} = M_{N \times 2}^{I} \times c_1 = \begin{bmatrix} Y_{11}^{I} & -Y_{12}^{I} \\ & \cdot \\ Y_{N1}^{I} & -Y_{N2}^{I} \end{bmatrix}. \tag{16}$$

to generate the combined data in the second unit, the spread data in (16) are grouped as (17):

$$\underbrace{D_I^0}_{Nx1} = \frac{\sum_{i=1}^{N} \left(M_{i1}^{I_0} + M_{i2}^{I_0} \right) + 1}{2} \qquad \underbrace{D_I^1}_{Nx1} = \frac{\sum_{i=1}^{N} \left(M_{i1}^{I_1} + M_{i2}^{I_1} \right) + 1}{2}. \tag{17}$$

Finally, the combined data is inserted to the decision block in order to recover the transmitted data. It should be emphasized that the decision block is uncomplicated, as illustrated in Figure. 3. The decision block will transform the data to one if it is larger than 0.5 and to zero in all other cases. Consequently, the suggested approach can send more data without increasing complexity.

3.3. MSTC-OFDM system model

The mathematical analysis of the proposed system (MSTC-OFDM) is presented in this subsection. Figure 4 depicts a generic block diagram of the MSTC-OFDM, which compresses symbol time and increases the data rate by using the MSTC at the transmitter and the MSTE at the receiver. The input data $(D_0, D_1, ..., D_N)$ is first processed by the MSTC block to compress the symbol time to one-fourth of its original length and increase capacity. Therefore, instead of utilizing one bit for each symbol, four bits are used. As a consequence, the MSTC block's output ranges from X_0 to $X_{N/4}$. The complex data symbol on the Kth sub-carrier is denoted by X_k, where $k = 1, 2, ..., N/4$. The $N/4$ resultant waveforms are transmitted into the $N/4$ input ports of an inverse fast Fourier transform (IFFT) block. Following IFFT, a discrete-time OFDM symbol is represented in the form:

$$x_k = \frac{2}{N} \sum_{m=0}^{\frac{N}{4}-1} X_m e^{j2\pi km/\frac{N}{4}}, \quad 0 \leq k \leq \frac{N}{4} - 1, \tag{18}$$

where k indicates the time index, N is indeed the number of sub-carriers, x_k is in fact the kth OFDM symbol, and X_m denotes the mth transferred data symbols. The generated time domain symbols are passed through a parallel-to-serial (P/S) converter. To ensure orthogonality and avoid ISI, a cyclic prefix (CP) of an appropriate

length (L_{cp}) is placed before each OFDM signal as a guard interval (GI) between OFDM symbols to mitigate the impact of multi-path propagation. The transmitted OFDM symbol with CP is written as (19):

$$x_k^{cp} = \frac{2}{N} \sum_{m=0}^{\frac{N}{4}-1} X_m e^{j2\pi km/\frac{N}{4}}, -L_{cp} \leq k \leq \frac{N}{4} - 1. \tag{19}$$

in order to retrieve the sent data, the transmitter procedures is effectively reversed in opposite order at the receiver side, as indicated in Figure 4.
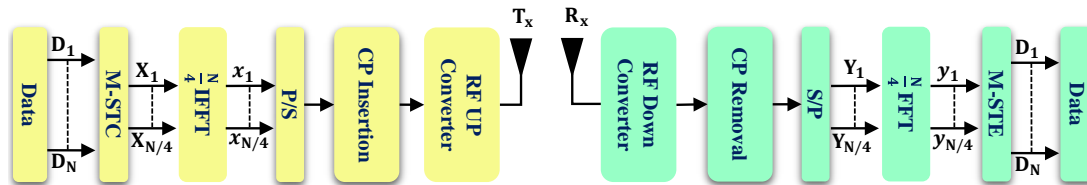

Figure 4. Block diagram of MSTC-OFDM system

4. SIMULATION RESULTS AND DISCUSSION

This part presents the numerical simulation results for the suggested method, including the performance metrics such as BER, OFDM symbol time, and power spectral density (PSD). The input data is modulated via binary phase-shift keying (BPSK) modulation. The bandwidth is 180 kHz, the Spacing frequency $\Delta f = 15$ kHz, the sampling frequency $f = 1.92$ MHz, the FFT size is 128, the CP = 1/4 of the OFDM symbol, and the model of the channel is additive white gaussian noise (AWGN). Using Monte-Carlo simulations, the BER is computed by totaling 1,000 OFDM symbols.

Figure 5 shows the performance comparison between the OFDM system using BPSK (BPSK-OFDM) and the MSTC-OFDM system based on the time domain of the transmitted signal. As shown in Figures 5(a) and 5(b), the MSTC-OFDM system reduces the OFDM symbol time to one-fourth compared to the BPSK-OFDM system. Consequently, employing the proposed approach saves 75% of the symbol time and can be exploited to transmit four times as much data as the BPSK-OFDM system.
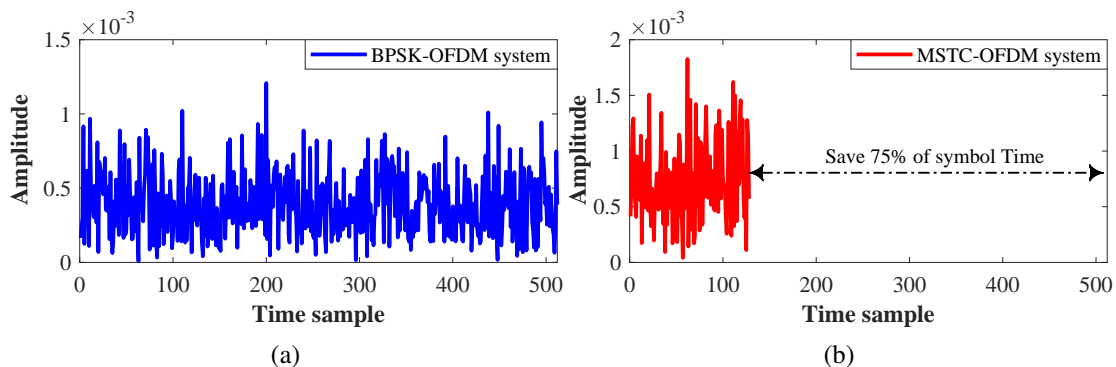

Figure 5. Performance comparison based on symbol time (a) BPSK-OFDM and (b) MSTC-OFDM systems

The spectra for three separate systems are shown in Figure 6. Figure 6(a) illustrates the spectrum of a BPSK-OFDM system, whereas Figure 6(b) depicts the spectrum of an HT-Fast-OFDM system, and Figure 6(c) displays the spectrum of the MSTC-OFDM system. It is obvious that all systems have the same bandwidth when parallel sinc pulses are employed as representations of 12 subcarriers for all systems. Despite having the same bandwidth as the BPSK-OFDM system, the HT-Fast-OFDM and MSTC-OFDM systems can transfer four times as much data compared to the BPSK-OFDM system. Unlike the HT-Fast-OFDM system, the MSTC-OFDM system does not modify the distance between the subcarriers, making it more resistant to ICI.

Figure 7 shows the power spectral density (PSD) for three different systems: the BPSK-OFDM system, the MSTC-OFDM system, and the HT-Fast-OFDM system. It can be seen clearly from Figure 7 that the three spectra occupy the same frequency range (approximately 180 kHz). However, when the three systems (BPSK-OFDM, HT-Fast-OFDM, and MSTC-OFDM) occupy the same bandwidth, the HT-Fast-OFDM system and the proposed MSTC-OFDM system have the ability to transmit four times the data as compared to the BPSK-OFDM system. Moreover, the MSTC-OFDM and the HT-Fast-OFDM systems do not affect the degradation of the bit error rate.
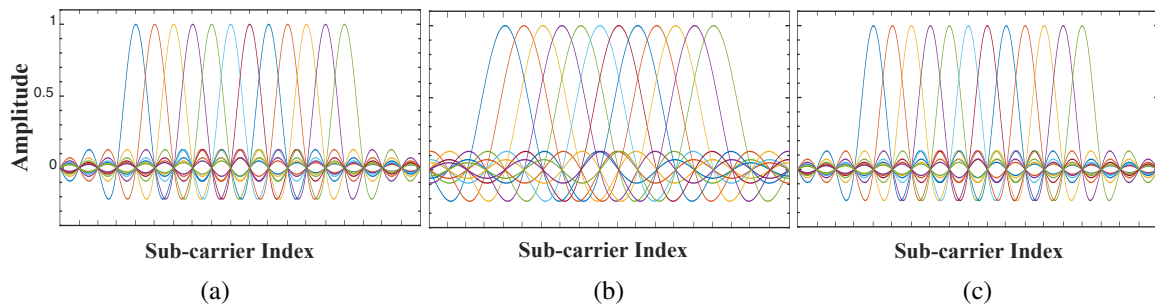
Figure 6. Sub-carriers representation for (a) BPSK-OFDM, (b) HT-Fast-OFDM [19], and (c) MSTC-OFDM
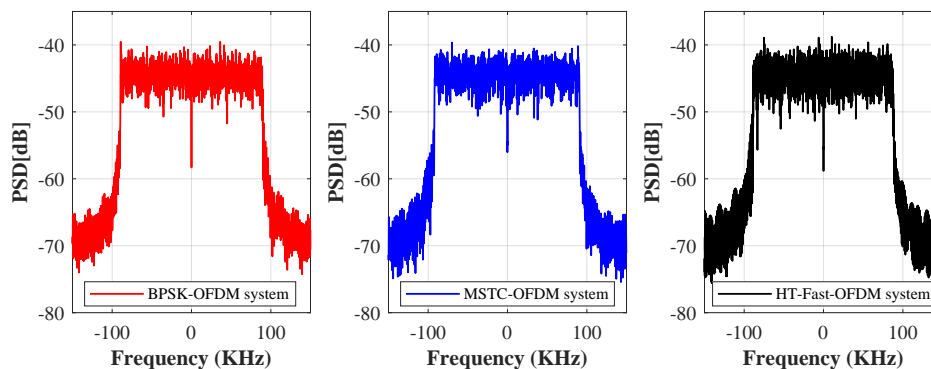
Figure 7. Comparison between BPSK-OFDM, MSTC-OFDM, and HT-Fast-OFDM [18] based on PSD

As mentioned in section 3, the proposed method can send four times as much data as a BPSK-OFDM system using the same bandwidth. Moreover, the BER is not degraded because the suggested method (MSTC-OFDM) uses one-dimensional modulation. Figure 8 compares OFDM BPSK, MSTC-OFDM, and HT-Fast-OFDM systems based on BER and data rate measurements. The two systems, MSTC-OFDM and HT-Fast-OFDM, can transfer four times more data than the BPSK-OFDM system; however, there is no degradation in the bit error rate, as illustrated in Figure 8(a). For the same BER ($BER = 10^{-4}$) and the same data rate, the signal-to-noise ratio (SNR) of the 16QAM-OFDM system is 12.3 dB, whereas the SNR of the MSTC-OFDM system is 8.4 dB. Therefore, the SNR gain while employing the MSTC-OFDM system is 3.9 dB. As a result, it may be concluded that the MSTC-OFDM system can transport data at a high rate while consuming less power.

It is clear from Figure 8(b) that the suggested MSTC-OFDM system has the same efficiency as the HT-Fast-OFDM and 16QAM-OFDM systems. The three systems can transmit 720 kbps at Eb/N0 = 10 dB, which is four times the data of the BPSK-OFDM system ($Rate_{BPSK-OFDM}$ = 180 kbps). Furthermore, the suggested system outperforms the 16QAM-OFDM system in terms of BER, as demonstrated in Figure 8(a), and outperforms the HT-Fast-OFDM system in terms of complexity.

4.1. Computational complexity

The complexity of BPSK-OFDM, MSTC-OFDM, and HT-Fast-OFDM is explained in this subsection. The FFT complexity for additions is N log2 N, whereas it is (N/2) log2 N for multiplication [25]. The following assumptions are applied to calculate complexity: i) the complexity of subtraction equals the complexity of

addition and ii) the complexity of division equals the complexity of multiplication. In the BPSK-OFDM system, it requires a total of $N\log_2(N)$ additions and $(N/2)\log_2(N)$ multiplications. The HT-Fast-OFDM system in [18] is divided into two units, each with N FFT points. The Hilbert transform pair, namely $g(t)$ and $\hat{g}(t)$, is multiplied by the two units. The first unit is multiplied by the Hilbert transform $g(t)$, while the second unit is multiplied by the Hilbert transform $\hat{g}(t)$. The two components are then joined. As a result, this system will require $N\log_2(N) + 2$ multiplications and $2N\log_2(N) + 1$ additions. The computational complexity of our suggested system (MSTC-OFDM) is as follows: in addition to the computational complexity of the BPSK-OFDM system, the MSTC technique requires $4N$ multiplication operations and $6N$ addition operations. As a result, the suggested approach, MSTC-OFDM, has a total of $(N/2)\log_2(N) + 4N$ multiplication operations and $N\log_2(N) + 6N$ addition operations. Table 1 highlights the computational complexity of the BPSK-OFDM, HT-Fast-OFDM, and MSTC-OFDM systems. It can be observed that the computational complexity of the suggested system, MSTC-OFDM, is lower than that of the HT-Fast-OFDM system.
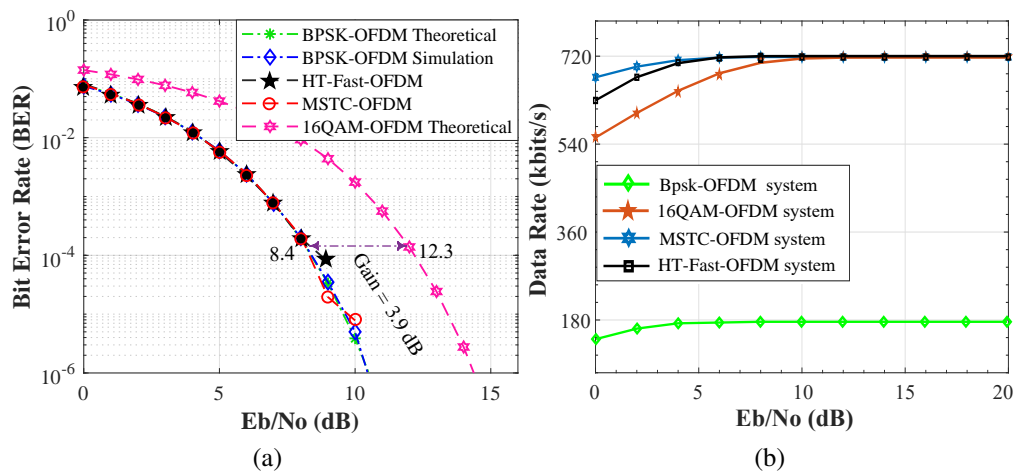

Figure 8. Comparison between BPSK-OFDM, MSTC-OFDM, and HT-Fast-OFDM [18] based on (a) BER and (b) data rate

Table 1. Computational complexity analysis

	BPSK-OFDM system		HT-Fast-OFDM system [18]		MSTC-OFDM system	
	No. Multiplications	No. Additions	No. Multiplications	No. Additions	No. Multiplications	No. Additions
N	$(N/2)\log_2(N)$	$N\log_2(N)$	$N\log_2(N) + 2$	$2N\log_2(N) + 1$	$(N/2)\log_2(N) + 4N$	$N\log_2(N) + 6N$
N=128	896	448	1793	898	1536	960
N=1024	10240	5120	20481	10242	15360	9216
N=4096	49152	24576	98305	49154	69632	40960

5. CONCLUSION

The MSTC technique is proposed in this article as a promising technique for 5G. This technique compresses the symbol time to one-fourth of its original length. According to simulation results, the proposed method (MSTC-OFDM) dramatically reduces the required time for each OFDM symbol by 75% when compared to a traditional OFDM system. This ultimately leads to an increase in capacity. The simulation results indicate that the proposed system (MSTC-OFDM) is equally efficient to the HT-Fast-OFDM and 16QAM-OFDM systems. Where the simulation results prove that the proposed system (MSTC-OFDM) can transmit data at the same rate (720 kbps) as the 16QAM-OFDM system, which is four times the rate of the BPSK-OFDM system (180 kbps). However, the suggested system outperforms the 16QAM-OFDM system in terms of BER, where the 16QAM-OFDM system requires an SNR that is 3.9 dB higher than the MSTC-OFDM system in order to achieve the same BER (BER = 10^{-4}). As a result, the MSTC-OFDM system can transfer the same amount of data as the 16QAM-OFDM system while consuming less power. In terms of computational complexity, the MSTC-OFDM outperforms the HT-Fast-OFDM system, while the BPSK-OFDM system outperforms the MSTC-OFDM. However, all three systems still have the same order of complexity $O(n)$.

REFERENCES

[1] V. Therrien, H. Mellah, V. Boutin, and B. Sansò, "A large-scale simulator for NB-IoT," *IEEE Access*, vol. 10, pp. 68231–68239, 2022, doi: 10.1109/ACCESS.2022.3186365.

[2] Y. Liu, Y. Deng, N. Jiang, M. Elkashlan, and A. Nallanathan, "Analysis of random access in NB-IoT networks with three coverage enhancement groups: a stochastic geometry approach," *IEEE Transactions on Wireless Communications*, vol. 20, no. 1, pp. 549–564, 2021, doi: 10.1109/TWC.2020.3026331.

[3] C. Zhang, M. Dong, and K. Ota, "Enabling computational intelligence for green internet of things: data-driven adaptation in LPWA networking," *IEEE Computational Intelligence Magazine*, vol. 15, no. 1, pp. 32–43, Feb. 2020, doi: 10.1109/MCI.2019.2954642.

[4] A. Parsa, T. A. Najafabadi, and F. R. Salmasi, "Implementation of smart optimal and automatic control of electrical home appliances (IoT)," in *2017 Smart Grid Conference (SGC)*, Dec. 2017, pp. 1–6, doi: 10.1109/SGC.2017.8308861.

[5] M. A. Desima, P. Ramli, D. F. Ramdani, and S. Rahman, "Alarm system to detect the location of IOT-based public vehicle accidents," in *2017 International Conference on Computing, Engineering, and Design (ICCED)*, Nov. 2017, pp. 1–5, doi: 10.1109/CED.2017.8308118.

[6] T.-Y. Yang, C.-S. Yang, and T.-W. Sung, "An intelligent energy management scheme with monitoring and scheduling approach for iot applications in smart home," in *2015 Third International Conference on Robot, Vision and Signal Processing (RVSP)*, Nov. 2015, pp. 216–219, doi: 10.1109/RVSP.2015.58.

[7] M. A. Obaidat, S. Obeidat, J. Holst, A. Al Hayajneh, and J. Brown, "A comprehensive and systematic survey on the internet of things: security and privacy challenges, security frameworks, enabling technologies, threats, vulnerabilities and countermeasures," *Computers*, vol. 9, no. 2, May 2020, doi: 10.3390/computers9020044.

[8] M. Dangana, S. Ansari, Q. H. Abbasi, S. Hussain, and M. A. Imran, "Suitability of NB-IoT for indoor industrial environment: a survey and insights," *Sensors*, vol. 21, no. 16, Aug. 2021, doi: 10.3390/s21165284.

[9] R. F. Sari, R. Harwahyu, and R.-G. Cheng, "Load estimation and connection request barring for random access in massive C-IoT," *IEEE Internet of Things Journal*, vol. 7, no. 7, pp. 6539–6549, Jul. 2020, doi: 10.1109/JIOT.2020.2968091.

[10] B. Su, Z. Qin, and Q. Ni, "Energy efficient uplink transmissions in LoRa networks," *IEEE Transactions on Communications*, vol. 68, no. 8, pp. 4960–4972, Aug. 2020, doi: 10.1109/TCOMM.2020.2993085.

[11] S. A. Gbadamosi, G. P. Hancke, and A. M. Abu-Mahfouz, "Building upon NB-IoT networks: a roadmap towards 5G new radio networks," *IEEE Access*, vol. 8, pp. 188641–188672, 2020, doi: 10.1109/ACCESS.2020.3030653.

[12] E. Rastogi, N. Saxena, A. Roy, and D. R. Shin, "Narrowband internet of things: a comprehensive study," *Computer Networks*, vol. 173, May 2020, doi: 10.1016/j.comnet.2020.107209.

[13] S. Kisseleff, J. Kneissl, G. Kilian, and W. H. Gerstacker, "Efficient detectors for telegram splitting-based transmission in low power wide area networks with bursty interference," *IEEE Transactions on Communications*, vol. 68, no. 12, pp. 7687–7701, 2020, doi: 10.1109/TCOMM.2020.3024203.

[14] E. M. Migabo, K. D. Djouani, and A. M. Kurien, "The narrowband internet of things (NB-IoT) resources management performance state of art, challenges, and opportunities," *IEEE Access*, vol. 8, pp. 97658–97675, 2020, doi: 10.1109/ACCESS.2020.2995938.

[15] S. Liu, L. Xiao, Z. Han, and Y. Tang, "Eliminating NB-IoT interference to LTE system: a sparse machine learning-based approach," *IEEE Internet of Things Journal*, vol. 6, no. 4, pp. 6919–6932, Aug. 2019, doi: 10.1109/JIOT.2019.2912850.

[16] A. Narayanan et al., "Collective intelligence using 5G: concepts, applications, and challenges in sociotechnical environments," *IEEE Access*, vol. 10, pp. 70394–70417, 2022, doi: 10.1109/ACCESS.2022.3184035.

[17] A. Hoglund et al., "Overview of 3GPP release 14 enhanced NB-IoT," *IEEE Network*, vol. 31, no. 6, pp. 16–22, Nov. 2017, doi: 10.1109/MNET.2017.1700082.

[18] X. Liu and I. Darwazeh, "Quadrupling the data rate for narrowband internet of things without modulation upgrade," in *2019 IEEE 89th Vehicular Technology Conference (VTC2019-Spring)*, Apr. 2019, pp. 1–5, doi: 10.1109/VTCSpring.2019.8746685.

[19] T. Xu and I. Darwazeh, "Uplink narrowband IoT data rate improvement: dense modulation formats or non-orthogonal signal waveforms?," in *2018 IEEE 29th Annual International Symposium on Personal, Indoor and Mobile Radio Communications (PIMRC)*, Sep. 2018, pp. 142–146, doi: 10.1109/PIMRC.2018.8580767.

[20] T. Xu and I. Darwazeh, "Non-orthogonal narrowband internet of things: a design for saving bandwidth and doubling the number of connected devices," *IEEE Internet of Things Journal*, vol. 5, no. 3, pp. 2120–2129, Jun. 2018, doi: 10.1109/JIOT.2018.2825098.

[21] T. Xu, C. Masouros, and I. Darwazeh, "Waveform and space precoding for next generation downlink narrowband IoT," *IEEE Internet of Things Journal*, vol. 6, no. 3, pp. 5097–5107, Jun. 2019, doi: 10.1109/JIOT.2019.2896724.

[22] M. S. El-Bakry, H. A. El-Shenawy, and A. E.-H. A. Ammar, "A time inversion and symbol time compression (TI-STC) scheme for ICI cancellation in high mobility OFDM systems," in *2017 Japan-Africa Conference on Electronics, Communications and Computers (JAC-ECC)*, Dec. 2017, pp. 82–85, doi: 10.1109/JEC-ECC.2017.8305779.

[23] A. Goldsmith, *Wireless communications*. Cambridge University Press, 2005.

[24] M. S. Elbakry, A. Mohammed, and T. Ismail, "Throughput improvement and PAPR reduction for OFDM-based VLC systems using an integrated STC-IMADJS technique," *Optical and Quantum Electronics*, vol. 54, no. 7, Jul. 2022, doi: 10.1007/s11082-022-03802-9.

[25] A. Mohammed, T. Ismail, A. Nassar, and H. Mostafa, "A novel companding technique to reduce high peak to average power ratio in OFDM systems," *IEEE Access*, vol. 9, pp. 35217–35228, 2021, doi: 10.1109/ACCESS.2021.3062820.

BIOGRAPHIES OF AUTHORS

Abdulwahid Mohammed 🆔 ⑧ SC ↻ received the B.S. degree in Electronics and Communication Engineering from Saad Dahlab University, Algeria, in 2010, and the M.S. degree in Electronics and Communication Engineering from Cairo University, Egypt, in 2019. During his Master's study, Abdulwahid worked as a research assistant in the Opto-Nanoelectronics Laboratory (One LAB), Department of Electronics and Communications, Faculty of Engineering, Cairo University, Egypt. He is currently pursuing the Ph.D. degree in Electronics and Communication Engineering from Al-Azhar University, Egypt. He is presently employed as a research assistant at the Smart Engineering Systems Research Center (SESC), Faculty of Engineering, Nile University, Egypt. His research interests include NB-IoT, wireless communication systems, 5G/6G communication networks, and artificial intelligence. He can be contacted at email: abdulwahid1520121@eng1.cu.edu.eg.

Hassan Mostafa 🆔 ⑧ SC ↻ received the B.Sc. and M.Sc. degrees (Hons.) in electronics engineering from Cairo University, Cairo, Egypt, in 2001 and 2005, respectively, and the Ph.D. degree in electrical and computer engineering from the Department of Electrical and Computer Engineering, University of Waterloo, Waterloo, ON, Canada, in 2011. He is currently an Associate Professor with the Nanotechnology and Nano-electronics Program, Zewail City of Science and Technology, Giza, Egypt, on leave from the Department of Electronics and Electrical Communications, Cairo University. He was an NSERC Postdoctoral Fellow with the Department of Electrical and Computer Engineering, University of Toronto, Toronto, ON, Canada. He was a Postdoctoral Researcher in collaboration with Fujitsu Research Laboratories in Japan and USA with a focus on the design of the next-generation FPGA. He has authored/coauthored more than 300 articles in international journals and conferences and five published books. His research interests include neuromorphic computing, the IoT hardware security, software-defined radio, reconfigurable low-power systems, analog-to-digital converters, low-power circuits, subthreshold logic, variation-tolerant design, soft error-tolerant design, statistical design methodologies, next-generation FPGA, spintronics, memristors, energy harvesting, MEMS/NEMS, power management, and optoelectronics. He has been a member of the IEEE Technical Committee of VLSI Systems and Applications since 2017. He was a recipient of the University of Waterloo SandFord Fleming TA Excellence Award in 2008, the Ontario Graduate Scholarship in 2009, the Waterloo Institute of Nano- Technology Nanofellowship Research Excellence Award in 2010, the Natural Sciences and Engineering Research Council of Canada Prestigious Postdoctoral Fellowship in 2011, and the University of Toronto Research Associate Scholarship in 2012. He can be contacted at email: hmostafa@uwaterloo.ca.

Abdelhady Abdelazim Ammar 🆔 ⑧ SC ↻ received the B.Sc. degree in Electronics and Communication Engineering from Alex University, Egypt, in 1963, the DEA and Ph.D. degrees from Paris University, France, in June 1965 and Dec 1968, respectively. He joined nuclear Engineering Department, in Madison Wisconsin, USA for two years from 1969 to 1971. He is a professor in Electronics and Communications Engineering department, Faculty of Engineering, Al-Azhar University, Cairo, Egypt since 1988. His research activities are within digital communications, mobile communications and digital signal processing. He can be contacted at email: hady42amar@gmail.com.